AAS 16-336

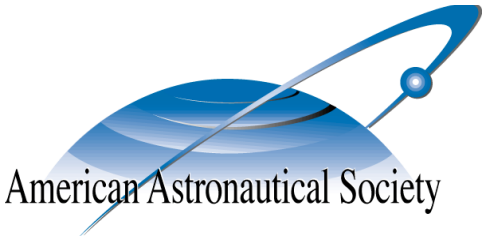

American Institute of
Aeronautics and Astronautics

RELATIVE MOTION ESTIMATION USING RECTILINEAR AND CURVILINEAR LINEARIZED RELATIVE ORBIT ELEMENTS

Trevor Bennett and Hanspeter Schaub

AAS/AIAA 26th Spaceflight Mechanics Meeting

Napa, California **February 14-18, 2016**

AAS Publications Office, P.O. Box 28130, San Diego, CA 92198

(Preprint) AAS 16-336

RELATIVE MOTION ESTIMATION USING RECTILINEAR AND CURVILINEAR LINEARIZED RELATIVE ORBIT ELEMENTS

Trevor Bennett* **and Hanspeter Schaub†**

Relative motion estimation finds application in space-based space situational awareness and proximity operations. Prior work demonstrates the capability and insight provided by a relative motion state vector chosen to be the Clohessy-Wiltshire integration constants, referred to as Linearized Relative Orbit Elements (LROEs). This study develops a curvilinear coordinate state vector and compares the estimation performance to both dimensional and non-dimensional rectilinear state estimation approaches. An Extended Kalman Filter (EKF) is developed to estimate the rectilinear and curvilinear LROE state and tested in an inertial simulation with bearings-only measurements and compared to bearings-plus-range filters. The curvilinear formulation demonstrates observability and improved estimation performance for the presented relative orbits. All LROE estimation approaches preserve much of the geometrical insight of the relative orbit while accommodating large initial condition errors.

INTRODUCTION

The growing utilization of Earth's orbits drives an increasing interest in and need for space situational awareness (SSA) and improved utilization. Satellite operators desire real-time knowledge of Earth-orbiting spacecraft and debris facilitated by quality measurements and robust propagation models. State information for orbiting objects can be acquired from inertial methods including ground based estimation and inertial differencing with GPS measurements[1,2] and space-fence installations. However, object measurements can also be captured by orbital platforms such as the Geosynchronous Space Situational Awareness Program (GSSAP) recently de-classified by the United States Air Force. In both ground-based and space-based systems, the goal of improved measurements and state estimation remains. In addition, several CubeSat missions have implemented relative motion control schemes that would benefit from the presented estimation approaches.[3–5] Direct estimation of the relative motion finds application in both SSA and proximity operation applications.

Exemplified by the GSSAP constellation, space-based observation platforms provide a complementary source of measurements for SSA applications. The space-based platforms utilize the more accurate knowledge of the observing craft and relative motion measurements to obtain the target object's state information. Prior work investigates the estimation of the relative motion through a variety of state descriptions. For example, one approach is to difference the orbit elements to derive new parameter sets.[1,6] Expressing the relative motion estimation in polar coordinates has also

*Graduate Research Assistant and NSTRF Fellow, Aerospace Engineering Sciences, University of Colorado.
†Alfred T. and Betty E. Look Professor of Engineering, Associate Chair of Graduate Affairs, Department of Aerospace Engineering Sciences, University of Colorado, 431 UCB, Colorado Center for Astrodynamics Research, Boulder, CO 80309-0431

been considered.[7] Further exploration has utilized curvilinear and nonlinear transformations of the linearized Cartesian motion. However, the formulations suffer from the same drawbacks of other relative motion descriptions.[8] To date the estimation methodology has assumed a Cartesian or orbit element difference state vector as outlined in Reference 9 including time-varying additional term derivations.

Critical circular orbit regimes, including the Geostationary belt or the International Space Station orbit, require great SSA attention. In cases where either observer or target is in a circular orbit, the Clohessy-Wiltshire (CW) equations describe the motion using time-varying Cartesian or curvilinear coordinates.[10] Research into using the CW equations for relative motion estimation has led researchers to derive new parameterizations.[6,11–13] An alternate approach to using the CW equations utilizes the invariants of the linearized CW equations as the state vector.[14] This method provides a constant relative motion state vector, or Linearized Relative Orbit Elements (LROEs), where the invariants provide relative orbit shape, orientation, and size. A relative motion estimation filter with a constant state vector benefits from epoch state filter efforts studied in Low-Earth Orbit (LEO) applications with substantial quality analysis techniques for the covariance.[15,16] Utilization of the invariant-inspired relative motion parameters exhibits exciting applications in relative motion sensing and control.

The angles-only relative motion estimation problem studied in References 1 and 17 is not fully observable using Cartesian formulations. Research in space-based observation in the GEO region highlights linearization error in the along-track relative coordinates.[18] Reference 19 discusses how curvilinear coordinates are superior to rectilinear coordinates in along-track estimation applications. First used for relative motion estimation in Reference 20, the present study extends the use of LROEs to curvilinear coordinates to combat the linearization error and improve observability. This following sections provide the development and demonstration of the LROE based extended Kalman filter for estimation using curvilinear LROE coordinates. Through inertial simulation and relative motion estimation, the non-singular LROEs and non-dimensional LROEs introduced in Reference 20 are compared to the presented curvilinear development. Considered are bearings-only measurement cases that demonstrate the weak observability gained by curvilinear coordinates and the bearings and range estimation required by the Cartesian formulation. Presented are the respective state vectors, filter formulations, and numerical simulations exhibiting the advantages of LROE state estimation and several state vector choices.

NONSINGULAR LROE SET

The relative motion of two satellites can be described by the inertial state vector difference in the deputy, or target, and chief. Consider the Hill frame defined in Figure 1.[21] The Clohessy-Wiltshire relative orbit equations can be derived from the Cartesian coordinates shown in Figure 1.[10] The state vector for Linearized Relative Orbit Element (LROE) estimation are the invariants of the CW equations. A slight modification to the CW equations removes the α and β ambiguity and largely preserves the inherent insight.[14] The ambiguity of the linear combination of A_0 and α, or B_0 and β, is removed in place of two perpendicular scaling terms. The modified non-singular LROE set

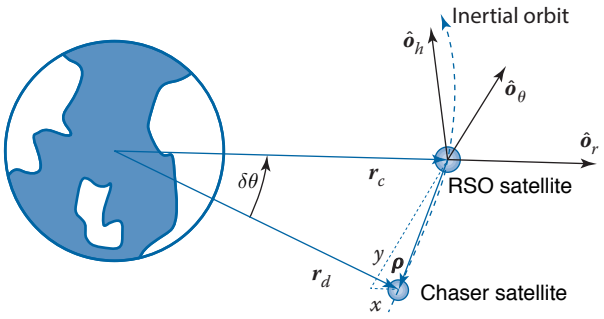

Figure 1. Local vertical local horizontal rotating Hill frame for formation flying.

therefore becomes

$$x(t) = A_1 \cos(nt) - A_2 \sin(nt) + x_{\text{off}} \tag{1a}$$

$$y(t) = -2A_1 \sin(nt) - 2A_2 \cos(nt) - \frac{3}{2} nt x_{\text{off}} + y_{\text{off}} \tag{1b}$$

$$z(t) = B_1 \cos(nt) - B_2 \sin(nt) \tag{1c}$$

The LROE form provides the relative motion geometry in the absence of perturbation. In the absence of perturbations, these parameters remain constant. The nominally invariant nonsingular LROE state vector $\boldsymbol{X}_{\text{NS}}$, is defined as

$$\boldsymbol{X}_{\text{NS}} = (A_1, A_2, x_{\text{off}}, y_{\text{off}}, B_1, B_2) \tag{2}$$

In the presence of perturbations, a Lagrangian Bracket formulation may be used to generate the specific LROE evolution equations.[14] The dynamics of the state vector are required for navigation filter applications. As described, the LROE set is considered to be invariant while the spacecraft pairs are influenced only by two-body gravitational effects. However, more accuracy to the dynamic modeling and filter applicability requires additional forces or perturbations to drive the LROE evolution. First derived in Reference 14, the dynamics of the LROE state can be obtained by applying Lagrange Brackets to the non-singular LROE equations. This approach is analogous to Lagrange's planetary equations in that the LROE set becomes osculating to match the perturbed relative orbit. The nonsingular state vector in Eq. (2) evolves according to Eq. (3) where $\boldsymbol{a}_d$ is the disturbance acceleration in the Hill frame.[14]

$$\dot{\boldsymbol{X}}_{\text{NS}} = \underbrace{\frac{1}{n} \begin{bmatrix} -\sin(nt) & -2\cos(nt) & 0 \\ -\cos(nt) & 2\sin(nt) & 0 \\ 0 & 2 & 0 \\ -2 & 3nt & 0 \\ 0 & 0 & -\sin(nt) \\ 0 & 0 & -\cos(nt) \end{bmatrix}}_{B(\boldsymbol{X},t)} \begin{bmatrix} a_x \\ a_y \\ a_z \end{bmatrix} \tag{3}$$

Eq. (3) is the variational equation of the non-singular LROE set, and is the relative motion equivalent of Gauss' variational equation for inertial orbital motion. Any perturbation or control accelerations can be applied to propagate the LROE variations. Recall that the CW equations already

account for two-body motion, so the differential perturbation accelerations can include drag, solar radiation pressure, and higher order gravity. Furthermore, the form in Eq. (3) is valid for both the rectilinear and curvilinear LROE formulations discussed in this manuscript. The matrix is derived from the CW form that all LROE state vectors utilize. Propagating the nonsingular Cartesian and curvilinear forms differ in the coordinitization of the acceleration vector.

REDUCED ORDER NON-DIMENSIONAL LROE SET

One of the challenges with bearings-only estimation is the lack of observability of the full relative motion state.[7,17] An example of the degenerate cases is the family of relative 2:1 ellipses where the bearings measurement history is the same for ellipses that only differ by a scale factor. This lack of knowledge regarding the scale factor is what introduces the lack of observability. Therefore, a non-dimensionalized LROE set is defined by dividing all the elements by a reference LROE element.[20] Without loss of generality, the A_1 term is selected for scaling to yield the reduced order non-dimensional LROE set[20]

$$\hat{\boldsymbol{X}} = \frac{1}{A_1}\begin{bmatrix} A_2 \\ B_1 \\ B_2 \\ x_{\text{off}} \\ y_{\text{off}} \end{bmatrix} = \begin{bmatrix} \hat{A}_2 \\ \hat{B}_1 \\ \hat{B}_2 \\ \hat{x}_{\text{off}} \\ \hat{y}_{\text{off}} \end{bmatrix} \tag{4}$$

Provided only the bearing measurements, the state vector provides the shape and orientation of the relative motion. Including range information would resolve the relative motion scale factor and provide the relative orbit size. The non-dimensional state equations follow as

$$x(t) = \cos(nt) - \hat{A}_2 \sin(nt) + \hat{x}_{\text{off}} \tag{5a}$$

$$y(t) = -2\sin(nt) - 2\hat{A}_2 \cos(nt) - \frac{3}{2} nt\hat{x}_{\text{off}} + \hat{y}_{\text{off}} \tag{5b}$$

$$z(t) = \hat{B}_1 \cos(nt) - \hat{B}_2 \sin(nt) \tag{5c}$$

with the non-dimensional state vector $\boldsymbol{X}_{\text{ND}}$, defined as

$$\boldsymbol{X}_{\text{ND}} = (\hat{A}_2, \hat{x}_{\text{off}}, \hat{y}_{\text{off}}, \hat{B}_1, \hat{B}_2) \tag{6}$$

This approach assumes that the non-dimensionalizing term is non-zero. If the filter does not know which terms are zero, a mixed-method of experts filtering approach would provide evidence of the correct formulation.

CURVILINEAR LROE COORDINATES

To help address the linearization errors and observability losses that plague the rectilinear form, the CW equations can also utilize a curvilinear formulation. Following the analytical form for rectilinear coordinates, the solution for the curvilinear position coordinates as a function of time is

$$\delta r(t) = C_0 \cos(nt + \alpha) + \delta r_{\text{off}} \tag{7a}$$

$$r_c \delta\theta(t) = -2C_0 \sin(nt + \alpha) - \frac{3}{2} nt\delta r_{\text{off}} + r_c \delta\theta_{\text{off}} \tag{7b}$$

$$z(t) = B_0 \cos(nt + \beta) \tag{7c}$$

Using the trigonometric expansion introduced in Reference 14, the nonsingular curvilinear position equations assume the form in Eq. (8) which is similar to the form in Eq. (1).

$$\delta r(t) = C_1 \cos(nt) - C_2 \sin(nt) + \delta r_{\text{off}} \tag{8a}$$

$$\delta s(t) = r_c \delta\theta(t) = -2C_1 \sin(nt) - 2C_2 \cos(nt) - \frac{3}{2} nt \delta r_{\text{off}} + r_c \delta\theta_{\text{off}} \tag{8b}$$

$$z(t) = B_1 \cos(nt) - B_2 \sin(nt) \tag{8c}$$

The advantage of the curvilinear coordinates is the nonlinear mapping back to Cartesian space that captures the arc of the orbit path. The ability to account for a curved path introduces weak observability for bearings-only estimation where the rectilinear formulation is not fully observable. For convenience, the chief orbit radius r_c is assumed known and the arc length curvilinear variable $\delta s_{\text{off}} = r_c \delta\theta_{\text{off}}$ is used. Utilizing the LROE approach, the curvilinear state vector $\boldsymbol{X}_{\text{C}}$, defined as

$$\boldsymbol{X}_{\text{C}} = (C_1, C_2, \delta r_{\text{off}}, \delta s_{\text{off}}, B_1, B_2) \tag{9}$$

EXTENDED KALMAN FILTER FORMULATION

An extended Kalman filter (EKF) is selected for the LROE state estimation. The choice of a nonlinear filter enables the nominal LROE set to vary more dramatically and converge given poor or no a priori. Furthermore, the EKF is a widely used filter and can be illustrative as a benchmark for the implementation of new relative orbit parameters.

General Filter Description

The LROE filter state is propagated forward in time using Eq. (10) where $\boldsymbol{F}$ are the modeled forcing functions. The dynamics are not constrained to be two-body admitting perturbations in the presented filter formulation. The LROE variational equations, for one state shown in Eq. (3), introduce a time-varying LROE set with filter-modeled perturbation forces

$$\dot{\boldsymbol{X}}_k = \boldsymbol{F}(\boldsymbol{X}(t_k), t_k) = B(\boldsymbol{X}(t_k), t_k)\boldsymbol{a}_d \tag{10}$$

where $B(\boldsymbol{X}(t_k), t_k)$ is defined by Eq. (3) and the disturbance acceleration is $\boldsymbol{a}_d$. The state covariance matrix is propagated forward using Eq. (11) requiring the state transition matrix $\Phi\left(t_k, t_{k-1}\right)$ and the addition of process noise $S(t)$.

$$\bar{P}_k = \Phi\left(t_k, t_{k-1}\right) P_{k-1} \Phi^T\left(t_k, t_{k-1}\right) + S(t) \tag{11}$$

The process noise matrix S is added at every time step to prevent filter saturation. The process noise for the current step is given by Eq. (12) where Q is the process noise covariance matrix.

$$\dot{S} = AS + SA + Q \tag{12}$$

The state covariance is updated using the Joseph formulation as shown in Eq. (13). The Joseph formulation of the covariance matrix is more consistently symmetric.

$$P_k = \left[I - K_k \tilde{H}_k\right] \bar{P}_k \left[I - K_k \tilde{H}_k\right]^T + K_k R_k K_k^T \tag{13}$$

Consistent with published EKF formulations, the measurement sensitivity matrix H is obtained by taking the partials of the observation with respect to the state vector.

$$H = \left[\frac{\partial \boldsymbol{G}(\boldsymbol{X}, t)}{\partial \boldsymbol{X}}\right]_i^* = \begin{bmatrix} \frac{\partial \text{Az}}{\partial \boldsymbol{X}} \\ \frac{\partial \text{El}}{\partial \boldsymbol{X}} \\ \frac{\partial \rho}{\partial \boldsymbol{X}} \end{bmatrix} \tag{14}$$

where $\boldsymbol{G}(\boldsymbol{X}, t)$ is the current vector of observations and $\boldsymbol{X}$ is the current LROE state.

An important implementation difference in the presented filter from the published EKF formulation is the inclusion of a perturbation to the estimated constant state.[15,22] Common between the epoch state filter and the LROE estimation filter is that the estimated state vector is constant. The concern with estimating a constant state vector is that the numerical implementation of the filter is capable of sticking to a particular, and often incorrect, state vector. Therefore, a full state of Gauss-Markov variables are propagated alongside the LROE state vector and are summed onto the LROE state immediately following the time update filter step. This perturbation is achieved from a random sample of a propagated Gauss-Markov process covariance and provides small magnitude alterations. The Gauss-Markov process is initialized from a random sample of the process noise covariance matrix.

Rectilinear State Measurement Model

The rectilinear filter implementation uses bearing and range measurement models described by

$$\text{Az}_{\text{exact}}(t) = \arctan\left(\frac{y(t)}{x(t)}\right) \tag{15a}$$

$$\text{El}_{\text{exact}}(t) = \arctan\left(\frac{z(t)}{\sqrt{x^2(t) + y^2(t)}}\right) \tag{15b}$$

$$\rho_{\text{exact}}(t) = \sqrt{x(t)^2 + y(t)^2 + z(t)^2} \tag{15c}$$

The bearing and range measurements can also be written in terms of the state vector variables by using the mappings provided by Eq. (1) for rectilinear coordinates. The H matrix using the non-singular rectilinear LROE form using the definitions in Eq. (1) for the azimuth measurement type is presented here with the partials for elevation and range measurements in the Appendix. The azimuth partials are

$$H_{1,1}(t) = \left(-2x(t)\sin(nt) - y(t)\cos(nt)\right)/\kappa_1 \tag{16a}$$

$$H_{1,2}(t) = \left(-2x(t)\cos(nt) + y(t)\sin(nt)\right)/\kappa_1 \tag{16b}$$

$$H_{1,3}(t) = \left(y(t) - \frac{3ntx(t)}{2}\right)/\kappa_1 \tag{16c}$$

$$H_{1,4}(t) = x(t)/\kappa_1 \tag{16d}$$

$$H_{1,5}(t) = 0 \tag{16e}$$

$$H_{1,6}(t) = 0 \tag{16f}$$

where

$$\kappa_1 = x^2(t) + y(t)^2 \tag{17a}$$

$$\kappa_2 = \sqrt{\kappa_1}\left(\kappa_1 + z^2(t)\right) \tag{17b}$$

The H matrix is the same for both rectilinear implementations of the filter with the non-dimensionalizing term column removed and the range row removed for the non-dimensional bearings-only case. The nominal EKF utilizes all 6 LROE states and has azimuth, elevation, and range measurements. However, the second case does not utilize range resulting in a 2×6 H matrix observability Grammian, $H^T H$, with only rank 5. Thus, the bearings-only filter formulation uses the 5 normalized states.

Curvilinear State Measurement Model

The curvilinear measurement equations require a nonlinear mapping from curvilinear coordinates to Cartesian coordinates as shown in Eq. (18). The mapping is not linearized. When introduced into the bearing measurement equations, the nonlinear curvilinear to rectilinear mapping is the source of obtaining weak observability. If Eq. (18) is linearized, then the curvilinear coordinates would not be fully observable. The mapping $r_c \delta\theta = y$ would make the observation sensitivity matrix for curvilinear coordinates reduce to the rectilinear form which would suffer from rank deficiency in the observability matrix.

$$x(t) = (\delta r + r_c)\cos(\delta\theta) - r_c \tag{18a}$$
$$y(t) = (\delta r + r_c)\sin(\delta\theta) \tag{18b}$$

Using the mapping in Eq. (18) and the time evolution of the curvilinear state in Eq. (8) , the measurement equations is written in terms of curvilinear coordinates.

$$\mathrm{Az}_{\mathrm{curv}}(t) = \arctan\left(\frac{(\delta r + r_c)\sin(\delta\theta)}{(\delta r + r_c)\cos(\delta\theta) - r_c}\right) \tag{19a}$$
$$\mathrm{El}_{\mathrm{curv}}(t) = \arctan\left(\frac{z(t)}{\sqrt{(\delta r + r_c)^2 - 2r_c(\delta r + r_c)\cos(\delta\theta) + r_c^2}}\right) \tag{19b}$$
$$\rho_{\mathrm{curv}}(t) = \sqrt{(\delta r + r_c)^2 - 2r_c(\delta r + r_c)\cos(\delta\theta) + r_c^2 + z(t)^2} \tag{19c}$$

The curvilinear state introduced in Eq. (9) contains sufficient nonlinearity to enable a rank 6 H matrix observability Grammian with bearings-only measurements. The curvilinear azimuth mea-

surement sensitivity is captured in

$$H_{1,1}^{\text{curv}}(t) = \left(-\cos\left(\frac{\delta s}{r_c}\right)\left[2(\delta r + r_c)x(t)\sin(nt) + r_c y(t)\cos(nt)\right] + \sin\left(\frac{\delta s}{r_c}\right)\left[r_c x(t)\cos(nt) - 2(\delta r + r_c)y(t)\sin(nt)\right]\right)/r_c\kappa_1 \tag{20a}$$

$$H_{1,2}^{\text{curv}}(t) = \left(-\cos\left(\frac{\delta s}{r_c}\right)\left[2(\delta r + r_c)x(t)\cos(nt) - r_c y(t)\sin(nt)\right] - \sin\left(\frac{\delta s}{r_c}\right)\left[r_c x(t)\sin(nt) + 2(\delta r + r_c)y(t)\cos(nt)\right]\right)/r_c\kappa_1 \tag{20b}$$

$$H_{1,3}^{\text{curv}}(t) = \left(-\cos\left(\frac{\delta s}{r_c}\right)\left[3ntx(t)(\delta r + r_c) + 2r_c y(t)\right] - \sin\left(\frac{\delta s}{r_c}\right)\left[3nty(t)(\delta r + r_c) - 2r_c x(t)\right]\right)/2r_c\kappa_1 \tag{20c}$$

$$H_{1,4}^{\text{curv}}(t) = (\delta r + r_c)\left(x(t)\cos\left(\frac{\delta s}{r_c}\right) + y(t)\sin\left(\frac{\delta s}{r_c}\right)\right)/r_c\kappa_1 \tag{20d}$$

$$H_{1,5}^{\text{curv}}(t) = 0 \tag{20e}$$

$$H_{1,6}^{\text{curv}}(t) = 0 \tag{20f}$$

where the terms $x(t)$ and $y(t)$ in both the H matrix and κ definitions are computed using Eq. (18). The elevation measurement sensitivity is detailed in the Appendix. However, the nonlinearity is small in the curvilinear H matrix which in turn requires large observational baselines to numerically capture the full rank of H. For small orbit trajectory curvature, the curvilinear measurement sensitivity collapses to the rectilinear form.

MEASUREMENT NOISE MODELS

Capitalizing on the LROE formulations, the proposed unperturbed filter formulation is an epoch state filter where the current measurement provides information that is mapped to a prescribed epoch. This filter considers the initialization time as the prescribed epoch although the epoch can be altered and reset as necessary. The noise on the measurements is accumulated from two sources. Simulating camera noise, a set of two first order Gauss-Markov variables are propagated and added onto the bearing measurements. In general practice, Gaussian white noise is added to all measurement types. Therefore the measurements provided to the filter are computed by Eq. (21).

$$\text{Az} = \text{Az}_{\text{exact}} + \sigma_{\text{Az}}^{GM} + w_{\text{Az}} \tag{21a}$$

$$\text{El} = \text{El}_{\text{exact}} + \sigma_{\text{El}}^{GM} + w_{\text{El}} \tag{21b}$$

$$\rho = \rho_{\text{exact}} + w_\rho \tag{21c}$$

The inclusion of the Gauss-Markov process more accurately represents the expected performance of a visual navigation camera and the white noise provides the random noise source. The first-order Gauss-Markov random walk process is propagated using the form

$$\dot{\boldsymbol{\sigma}} = -B_{\text{GM}}\boldsymbol{\sigma} + W_k \tag{22}$$

where the B matrix provides the time-constant-drive decay of the current variable value. The white noise process matrix W_k is a randomly sampled value from a camera specific error covariance W.

The time constants for the camera considered are 15 minutes such that the Gauss-Markov B matrix is given by

$$B_{\text{GM}} = \begin{bmatrix} 1/\tau_{\text{Az}} & 0 \\ 0 & 1/\tau_{\text{El}} \end{bmatrix} \tag{23}$$

The W matrix is the diagonal covariance of the camera white noise with elements w_{cam}. The camera considered in this study is a 5 mega-pixel, $n_{\text{p}} = 5 \times 10^6$, camera. The noise w_p is assumed to be about 0.05 pixels for 3σ error. The camera is assumed to have a more narrow field of view with a half angle of $\alpha = 10^\circ$. This gives the radian noise magnitude of

$$w_{\text{cam}} = \frac{w_p}{n_{\text{p}}} * 2\alpha \tag{24}$$

The measurement noise for the azimuth and elevation measurements are computed similarly with the range error scaled by the observational baseline.

$$w_{\text{az}} = w_{\text{el}} = \frac{w_m}{n_{\text{p}}} * 2\alpha \tag{25a}$$

$$w_\rho = \rho * \tan\left(\frac{w_r}{n_{\text{p}}} * 2\alpha\right) \tag{25b}$$

where w_m is 0.3 pixels for 3σ error and w_r is 1.5 pixels for 3σ error. These levels of accuracy are possible with modern camera technology and enable the curvilinear formulations. The noise parameters included provide a more realistic benchmark for the LROE EKF formulation.

ILLUSTRATIVE RECTILINEAR LROE ESTIMATION CASES

Of interest is the ability to estimate the relative motion of a target orbital object from a series of space-based observations. The Linearized Relative Orbit Element (LROE) set is well suited to the space-based observation application because the formulation is derived from formation flying. The LROE extended Kalman filter formulation is implemented in a numerical simulation to demonstrate the feasibility and simplicity of estimating the LROE relative orbit given minimal sensor information. Motivated by observations of orbital platforms, one case compares bearings-only measurements with the case augmented by object centroid range measurements. The observations are extracted every 3 seconds from simulated true positions and are then altered by the addition of sensor noise as described in previous sections. The camera noise is defined in Eq. (24) and has a value of 1.56×10^{-5} radians and a nominal range error of 2 centimeters at 200 meter range. To improve filter behavior, a measurement noise under-weighted to 5 times the true noise value as a preliminary filter tuning. The two satellites are inertially propagated with the full nonlinear two-body dynamics and are currently without perturbations. However, additional perturbations are easily included given the LROE dynamics provided by the Lagrangian Brackets.

The chief spacecraft is initialized with a semi-major axis of 7500 kilometers and all other orbit elements as zero. The true relative orbit is initialized with $\boldsymbol{X}^{\text{true}}$ and the filter is given the initial conditions $\boldsymbol{X}^{\text{true}} + \Delta\boldsymbol{X}$. The LROE filter is applied to a drifting target satellite defined by the

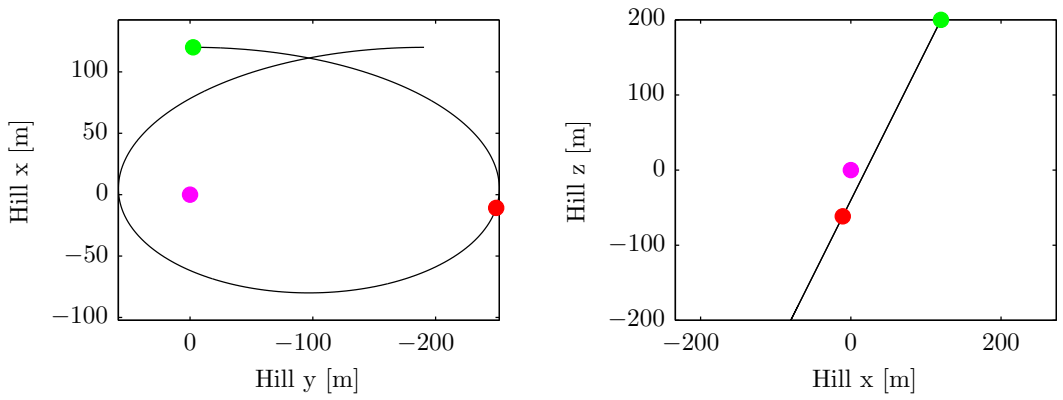

(a) Relative orbit, planar projection.

(b) Relative orbit, XZ projection.

Figure 2. Hill frame relative orbit for the drifting relative ellipse example case. Start at o, finish at o about the chief.

Cartesian initial conditions and filter state error as

$$\boldsymbol{X}^{\text{true}} = \begin{bmatrix} A_1 \\ A_2 \\ x_{\text{off}} \\ y_{\text{off}} \\ B_1 \\ B_2 \end{bmatrix} = \begin{bmatrix} 100 \\ 0 \\ 20 \\ \text{-}2.5 \\ 200 \\ 0 \end{bmatrix} \text{[m]} \qquad \Delta\boldsymbol{X} = \begin{bmatrix} 10 \\ \text{-}2 \\ 5 \\ \text{-}5 \\ \text{-}7 \\ 2 \end{bmatrix} \text{[m]} \tag{26}$$

The true drifting relative orbit over a simulated full orbit is shown in Cartesian Hill frame coordinates in Figure 2 with the filter cutoff at 0.3 orbits shown in red. The presented Hill frame relative orbit is the basis for comparing three numerical simulation cases. The first case demonstrates the bearings and range LROE estimation. The second case demonstrates bearings-only with the non-dimensional LROE set. The final case introduces curvilinear bearings-only estimation and compares the resulting quality to the two rectilinear cases.

LROE Relative Orbit Estimation using Bearings and Range

Recall that the CW equations provide the relative motion of a target in Cartesian coordinates as a function of the LROE state. The full LROE state estimation requires bearings and range measurements as required to maintain full rank in the observation sensitivity matrix H. Consider first the case where the full rectilinear state is estimated with bearings and range measurements. In the absence of perturbations, the LROE state is constant and can therefore converge with large initial condition errors. To allow for large initial condition errors, such as the 200% error on y_{off} term, the initial filter covariance is exaggerated to $P_0 = 10^{10} \times \text{diag}[1,\ 1,\ 1,\ 1,\ 1,\ 1]$ which also provides ample buffer with the 1 km range of greatest validity inherent in the CW equations. The filter process noise is

$$Q^{\text{est}} = 0.005 \times \text{diag}[1,\ 1,\ 10,\ 1,\ 1,\ 1]$$

The magnitude of the process noise is sufficiently large such that the covariance bounds in the estimate encapsulate the state errors.[20] The process noise term on the x_{off} term is increased to an

order of magnitude larger than the terms for other states. This linearization required to obtain the CW equations in the Cartesian frame introduce most of the truncation error into the x_{off} term and so the filter will require greater estimate flexibility in this state variable.

The EKF LROE filter using bearings and range with the initialized state and error detailed in Eq. (26) achieves a final state error of

$$\Delta \boldsymbol{X}_{\text{final}} \approx [-0.0009,\ 0.04,\ 0.007,\ -0.001,\ -0.04,\ -0.09]\ [\text{m}]$$

after only 0.3 orbits. The convergence of each state variable over the 0.3 orbits is shown in Figure 3. As desired, the covariance remains sufficiently open due to the larger initial covariance, sufficient process noise, and the camera Gauss-Markov time constant of 15 minutes. Due to the visualized scale, the covariance pinch at 0.25 orbits is not clearly visible in the A_1 state shown in Figure 3(a) and the B_2 state shown in Figure 3(f). However, the presence of the narrowed covariance around 0.25 orbits suggests a filter that has a reasonable process noise magnitude.

The pre- and post-fit residuals for the estimated LROE state are shown in Figure 4. Inspection of the pre-fit residuals reveals the desired trend towards residual noise at the magnitude of the visual sensor capability. The lack of definitive character in the residuals confirms the state estimate is reasonable and is unlikely to be refined further.

The presented LROE filtering pass only utilizes 0.3 relative orbits to converge to a reasonable answer. This speed of convergence from large initial condition errors is advantageous for space-to-space based observations because only fractions of an orbit are required to achieve the estimate. The filter results presented in Figures 3 and 4 demonstrate the capability of a LROE state vector in relative motion estimation. However, the range observation may not always be possible or may not be of sufficient accuracy. This leads to estimation approaches that consider bearings-only measurements.

Relative Orbit Estimation using the Reduced Non-Dimensional LROE Set

Consider the case where the range measurement cannot be accurately determined from visual sensor data. This is possible when the filter possesses a poor target object geometrical or lighting model to compare against the visual observation. Therefore, the LROE state is applied to the bearings-only sensor scenario. A numerical simulation of the non-dimensional LROE set with A_1 as the non-dimensionalizing term. The following example shows the ability to estimate the shape and orientation of the relative orbit using bearings-only measurements.

The initial filter covariance is given by $P_0 = 10^3 \times \text{diag}[1,\ 1,\ 1,\ 1,\ 1]$ which is sufficient for the states that have been normalized by relative orbit size. The filter process noise is

$$Q^{\text{est}} = 0.005 \times \text{diag}[1,\ 10,\ 1,\ 1,\ 1]/|A_1|$$

where the x_{off} term retains the order of magnitude increase in process noise. Given the linearization error and the larger process noise requirements for x_{off}, it is recommended that the non-dimensional LROE state not use x_{off} as the non-dimensionalizing term.

The non-dimensional estimation output is re-dimensionalized by the A_1 scaling term to better illustrate the convergence and compare against other filter outputs. In general, the filter does not have knowledge of the scaling term and converges to the correct non-dimensional LROE states. The final state estimate error after 0.3 chief orbits is reduced to

$$\Delta \boldsymbol{X}_{\text{final}} = [0.003,\ -0.09,\ 0.007,\ 0.006,\ 0.09]\ [\text{m}] \tag{27}$$

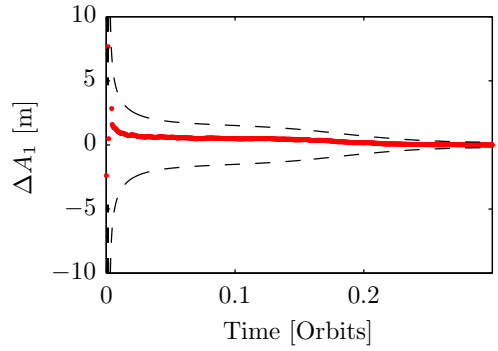

(a) A_1 state and 3σ variance.

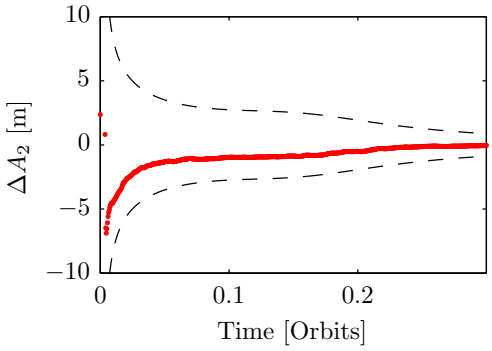

(b) A_2 state and 3σ variance.

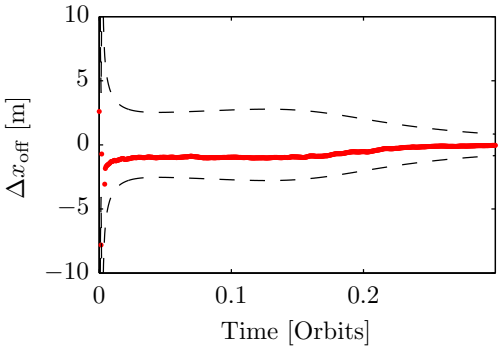

(c) x_{off} state and 3σ variance.

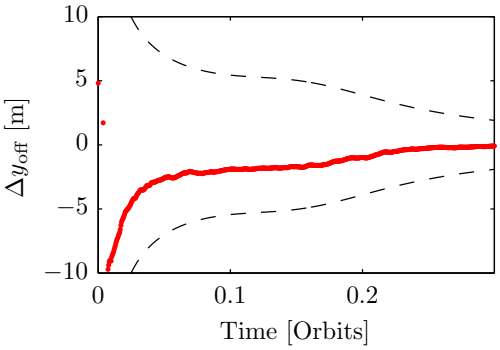

(d) y_{off} state and 3σ variance.

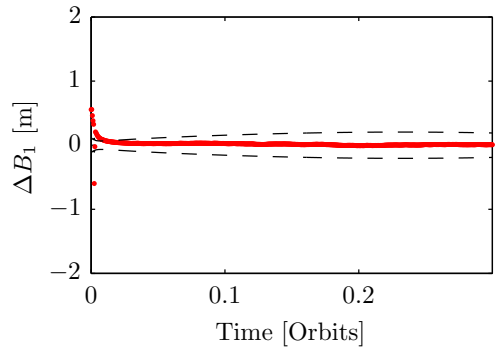

(e) B_1 state and 3σ variance.

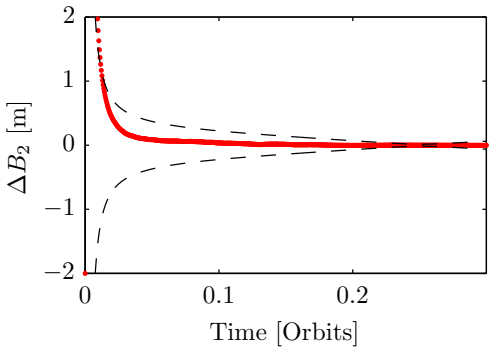

(f) B_2 state and 3σ variance.

Figure 3. LROE estimated state error and covariance envelopes demonstrating full relative motion estimation for LROEs.

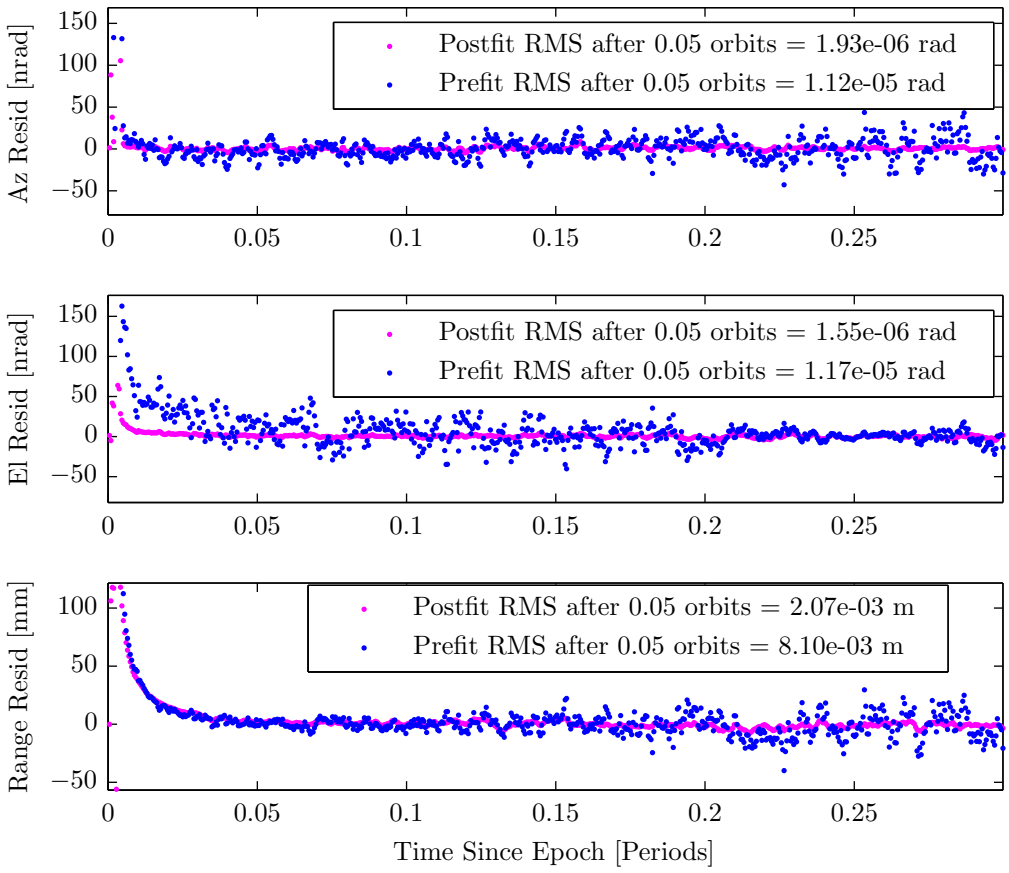

Figure 4. Estimation pre- and post-fit residuals for the full rectilinear LROE set.

after 0.3 orbits. The re-dimesionalized filter state estimates over the considered 0.3 orbits are shown in Figure 5. The A_1 term is used for normalization and therefore is not included in the filter formulation other than to re-dimensionalize the state estimate. The covariance envelopes are sufficiently open during the initial observations to accommodate large initial condition errors and then sufficiently reduces for the estimate to converge on the truth. As can be seen in all states in Figure 5, the better observational geometry in B_2 that reduces the covariance in Figure 5(d), lends to the convergence of all states. This supports that the observational window must be large enough to get significant geometry change despite the speed of convergence on the LROE state that is not as apparent in the full state estimation shown in Figure 3. In general, the LROE state will require more than 0.25 orbits to pass through critical observational geometry points. The filter state estimate is quite accurate with errors on the order of the full state estimate. The convenient geometric insight obtained when performing relative motion estimation using the LROEs although is limited by lack of scale knowledge. Recall, given the non-dimensional states in Eq. 6 the output estimate describes the relative orbit shape and orientation but not size.

The measurement residuals for the non-dimensional LROE state estimation are shown in Figure 6. As desired, the pre-fit residuals tend towards zero-mean noise at the resolution of the sensor noise.

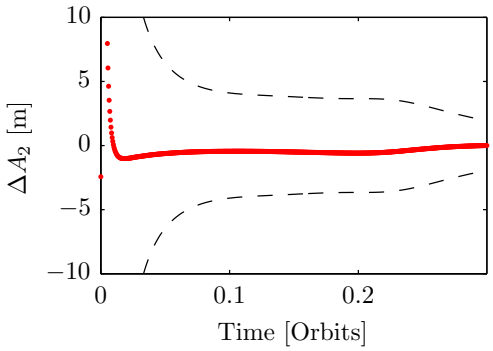

(a) A_2 state and 3σ variance.

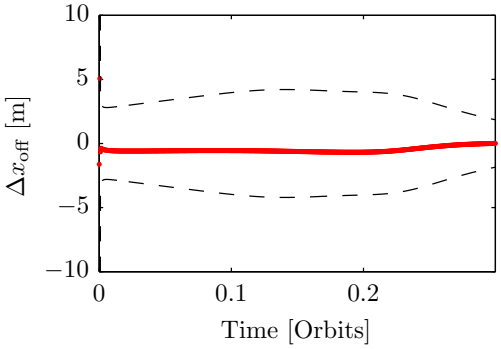

(b) x_{off} state and 3σ variance.

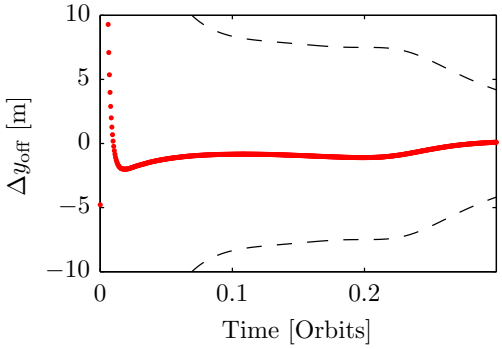

(c) y_{off} state and 3σ variance.

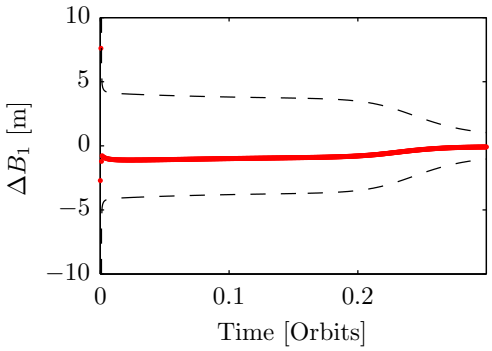

(d) B_1 state and 3σ variance.

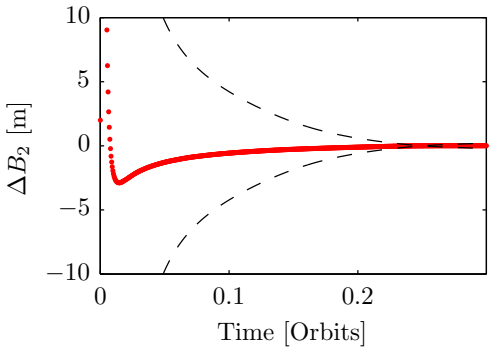

(e) B_2 state and 3σ variance.

Figure 5. LROE estimated state error and covariance envelopes demonstrating bearings-only relative motion estimation for non-dimensionalized LROEs after re-dimensionalizing by the A_1 scaling term.

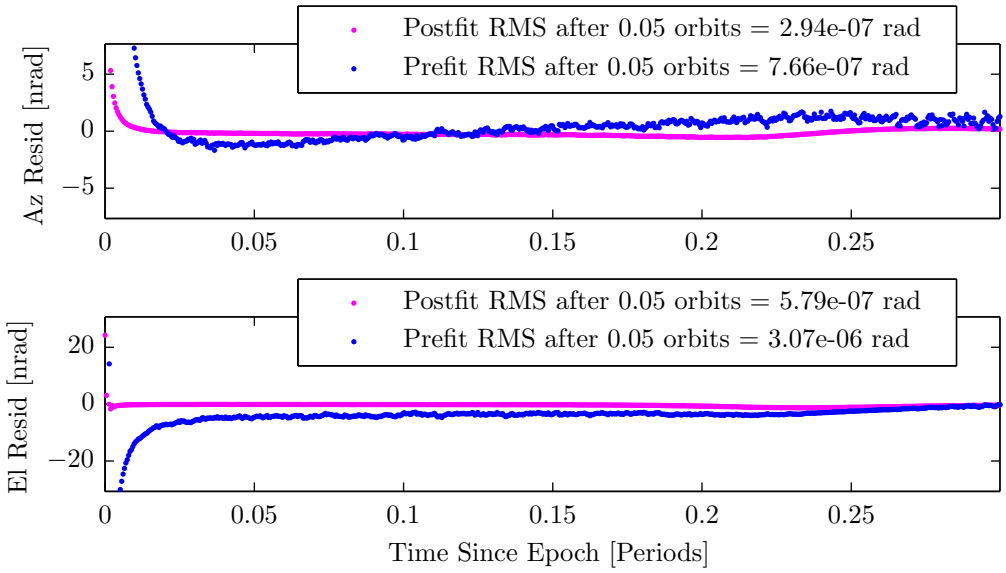

Figure 6. Estimation pre- and post-fit residuals for the non-dimensional rectilinear LROE set after re-dimensionalizing by the A_1 scaling term.

The non-dimensional residuals are more compact than the full state residuals shown in Figure 4. Two factors that contribute to the improved non-dimensional residuals are that the state is non-dimensional and that the filter is fitting to fewer measurements that are bearings-only.

The results provided by the non-dimensional bearings-only and the dimensional rectilinear state estimation simulations clearly demonstrate the feasibility of using LROEs for space-to-space based relative motion estimation. The rectilinear examples shown only demonstrate feasibility within a range of 1 kilometer from the chief. Recall that the CW equations make linearizing assumptions to obtain the desired form thereby limiting use over larger relative orbits. As detailed previously, the curvilinear form of the CW equations provides a solution valid over large relative orbits.

CURVILINEAR LROE RELATIVE ORBIT ESTIMATION

The validity of the curvilinear form over large relative orbits strongly justifies use of the curvilinear LROE state. Further, as described in the development of the EKF, the curvilinear form also benefits from a full rank measurement sensitivity matrix with bearings-only measurements. To capture the full rank measurement sensitivity, the relative motion baseline is increased such that the drifting target is initialized with the state

$$\boldsymbol{X}^{\text{true}} = \begin{bmatrix} C_1 \\ C_2 \\ \delta r_{\text{off}} \\ \delta s_{\text{off}} \\ B_1 \\ B_2 \end{bmatrix} = \begin{bmatrix} 10000 \\ 0 \\ 2000 \\ \text{-}250 \\ 20000 \\ 0 \end{bmatrix} \text{[m]} \qquad \Delta\boldsymbol{X} = \begin{bmatrix} 1000 \\ \text{-}200 \\ 500 \\ \text{-}500 \\ \text{-}700 \\ 200 \end{bmatrix} \text{[m]} \tag{28}$$

The relative state is initialized to be approximately 100 times the rectilinear case such that the curvature of the relative orbit becomes significant. The relative orbit is shown for a single chief

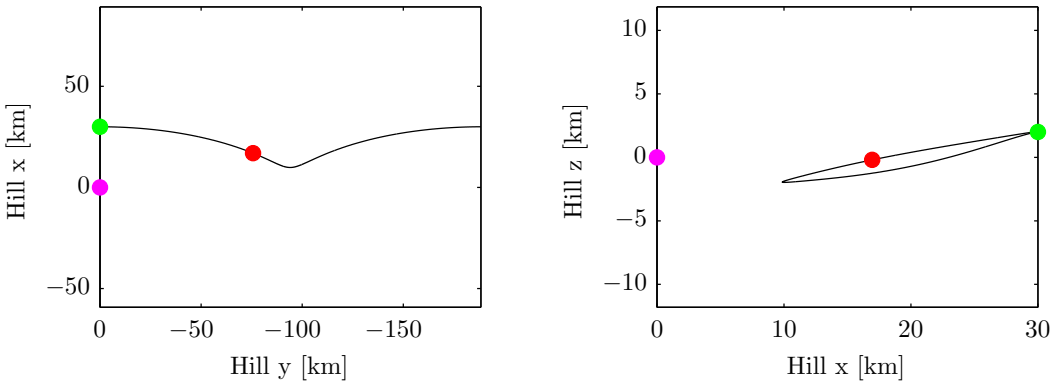

(a) Relative orbit, planar projection.

(b) Relative orbit, XZ projection.

Figure 7. Hill frame relative orbit for the curvilinear drifting relative ellipse example case. Start at o, finish at o about the chief.

orbit period in Figure 7. There is sufficient change in geometry in the Hill frame plane, however, the flattening of the out-of-plane motion will influence the relative motion filter performance.

The initial filter covariance is given by $P_0 = 10^1 7 \times \text{diag}[1,\ 1,\ 1,\ 1,\ 1]$ which is largely inflated for the scale of the relative orbit problem. The filter process noise is

$$Q^{\text{est}} = 0.25 \times \text{diag}[1,\ 1,\ 10,\ 10,\ 1,\ 1]$$

producing the final state estimate error after 0.3 chief orbits of

$$\Delta \boldsymbol{X}_{\text{final}} = [337.1,\ 5.9,\ 74.4,\ 40.2,\ 643.0,\ -1.0]\ [\text{m}] \tag{29}$$

The filter state estimates over the considered 0.3 orbits are shown in Figure 8. Most notable is the lack of estimate improvement in the B_1 term. Referring back to Figure 7, the flattening of the out-of-plane motion manifests in poor measurement geometry for B_1, shown in Figure 8(f), during the first 0.3 chief orbits. However, additional estimation time would improve this result as the target object would move closer and provide better observational geometry as the target approached the half-orbit point. Inspection of Figure 8(a) reveals that the estimate approaches the covariance envelope bound. The combination of these two estimates suggests that the EKF is approaching numerical implementation challenges. The scale of the curvilinear relative orbit estimation problem approaches the limit of the numeric validity of the EKF. The large length scales and accurate measurements may cause numeric instability in the propagation of the covariance and therefore the state update.[22] Alternate filter types that implement square root covariance propagation, such as the square root information filter, may provide greater numerical stability over a larger range of curvilinear state vectors.

Not surprisingly, the measurement residuals demonstrate some underlying character that is not purely noise. Considering that the filter estimate did not completely converge due to numerical limitations and observational geometry, the residuals suggest that the estimate is approaching reasonable but requires further refinement.

The curvilinear LROE state estimate is shown to provide an overall reduction in large initial condition errors and is applicable to both large and small relative states. In the case where the

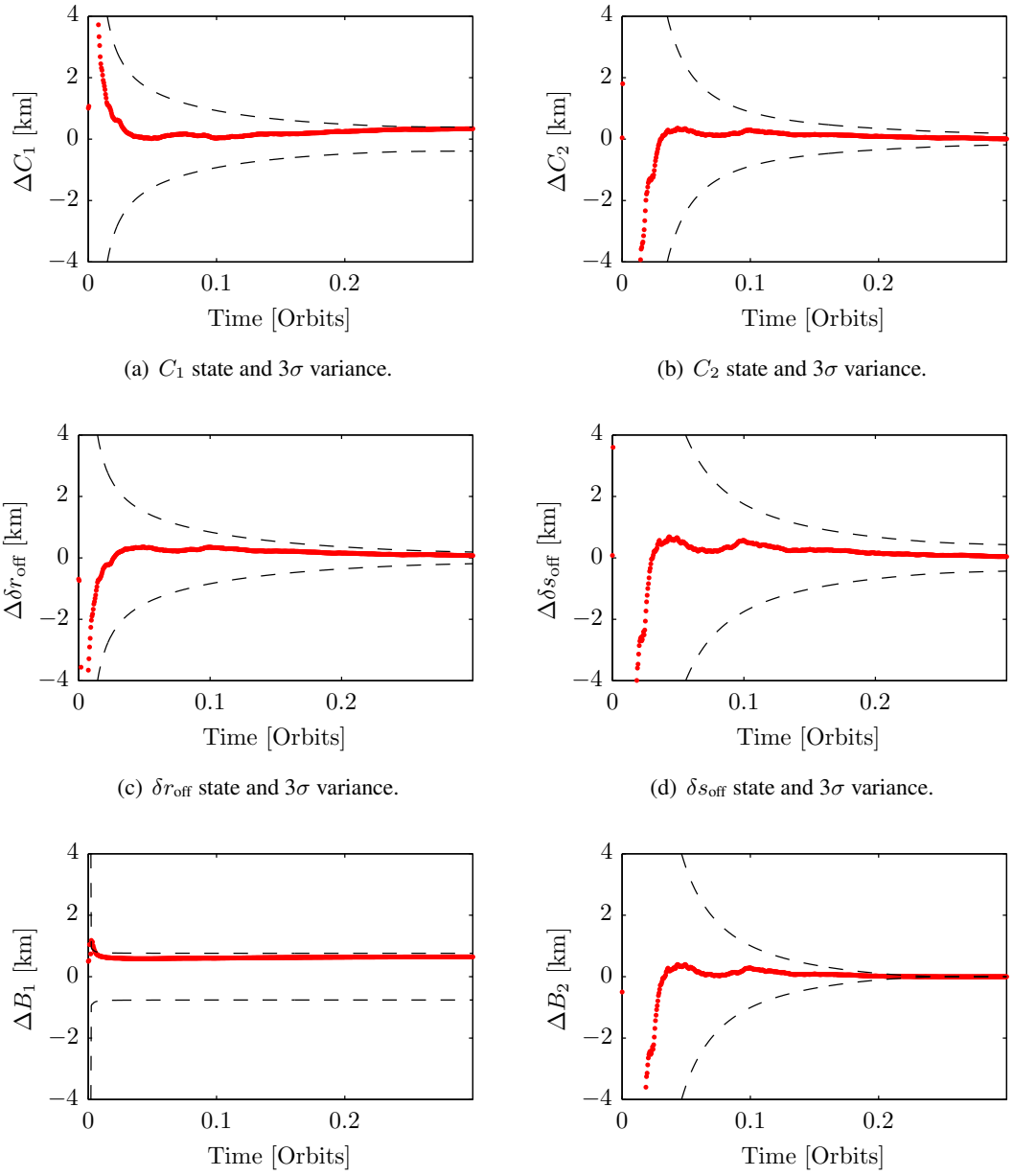

(a) C_1 state and 3σ variance.

(b) C_2 state and 3σ variance.

(c) δr_{off} state and 3σ variance.

(d) δs_{off} state and 3σ variance.

(e) B_1 state and 3σ variance.

(f) B_2 state and 3σ variance.

Figure 8. LROE estimated state error and covariance envelopes demonstrating full relative motion estimation for LROEs.

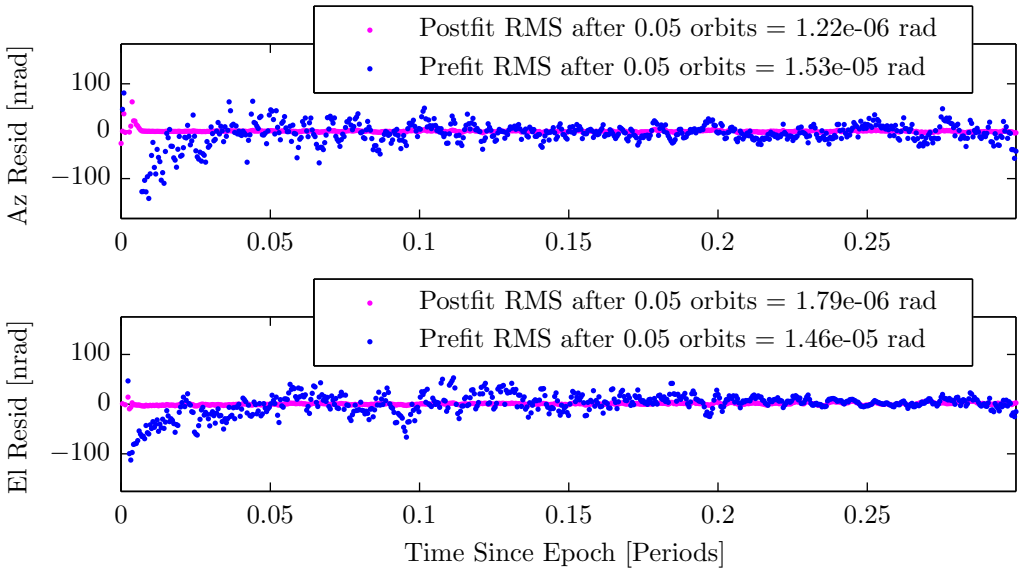

Figure 9. Estimation pre- and post-fit residuals for the curvilinear LROE set.

relative orbit dimension approaches the length scale of the rectilinear cases presented, the numerical or measurement precision is not accurate enough to retain the full rank measurement sensitivity. Therefore, the curvilinear form should be reserved for large relative orbits and the more simple rectilinear form for small relative orbits. The curvilinear form does provide further capability in that the state is fully observable with bearings-only measurements. To take advantage of this capability, the relative orbit must be large or the measurement capability precise to take advantage of the curvilinear form. However, if the curvilinear form is used significantly larger relative orbits, a more stable covariance update formulation is required.

CONCLUSIONS

The presented Linearized Relative Orbit Element (LROE) state derived from the Clohessy-Wiltshire equations provides an insightful and elegant propagation formulation that is applicable to filter. An extended kalman filter (EKF) is formulated for LROE estimation and several numerical examples demonstrate the feasibility of an LROE approach. The EKF rectilinear relative motion estimates provide centimeter to millimeter level accuracy in fractions of the chief relative orbit. To address the lack of range measurements and the challenge of bearings-only measurements, a non-dimensional LROE state and filter results are presented. For larger relative orbits, the curvilinear LROE form provides full state observability with bearings-only measurements and greater fidelity with additional measurements. If the relative orbit size exceeds the dimension presented in this manuscript, an alternate to the EKF should be implemented.

ACKNOWLEDGEMENTS

The authors would like to thank the NASA Space Technology Research Fellowship (NSTRF) program, grant number NNX14AL62H, for support of this research.

REFERENCES

[1] S. D. G. Gaias and J. S. Ardaens, "Angles-Only Navigation to a Noncooperative Satellite Using Relative Orbit Elements," *Journal of Guidance, Control, and Dynamics*, Vol. 37, No. 2, 2014.

[2] E. Gill, S. D'Amico, and O. Montenbruck, "Autonomous Formation Flying for the PRISMA mission," *AIAA Journal of Spacecraft and Rockets*, Vol. 44, May–June 2007, pp. 671–681.

[3] S. D. Amico, J. S. Ardaens, and R. Larsson, "In-flight demonstration of formation control based on relative orbit elements," *4th International Conference on Spacecraft Formation Flying Missions and Technologies*, August 18-20 2011.

[4] J. Schwartz and T. Krenzke, "Error-contracting impulse controller for satellite cluster flight formation," *AIAA Guidance, Navigation and Control Conference*, Boston, MA, August 19-22 2013.

[5] S. Chalt and D. A. Spencer, "PROX-1: Automated Trajectory Control for ON-Orbit Inspection," *37th Annual American Astronautical Society Guidance and Control Conference*, January 2014.

[6] F. R. Chavez and T. A. Lovell, "Relative-Orbit Element Estimation for Satellite Navigation and Guidance," Providence, RI, AIAA/AAS Astrodynamics Specialist Conference and Exhibit, August 16-19 2004.

[7] V. J. Aidala and S. E. Hammel, "Utilization of Modified Polar Coordinates for Bearings-Only Tracking," *IEEE Transactions on Automatic Control*, Vol. AC-28, March 1983.

[8] A. C. Perez and T. A. Lovell, "Nonlinear representations of satellite relative motion equations using curvilinear transformations," *AAS*, 2015.

[9] T. A. Lovell and D. A. Spencer, "Relative Orbital Elements Formulation Based upon the Clohessy-Wiltshire Equations," *Journal of Astronautics*, February 2015.

[10] W. H. Clohessy and R. S. Wiltshire, "Terminal Guidance System for Satellite Rendezvous," *Journal of the Aerospace Sciences*, Vol. 27, Sept. 1960, pp. 653–658.

[11] T. A. Lovell and S. G. Tragesser, "Guidance for relative motion of Low Earth Orbit spacecraft base on relative orbit elements," *AIAA/AAS Astrodynamics Specialist Conference*, Providence, Rhode Island, August 16-19 2004.

[12] T. A. Lovell, S. G. Tragesser, and M. V. Tollefson, "A practical guidance methodology for relative motion of LEO spacecraft base on the Clohessy-Wiltshire equations," *14th AAS/AIAA Spaceflight Mechanics Meeting*, Maui, Hawaii, February 8–12 2004.

[13] S. D. Amico, E. Gill, and O. Montenbruck, "Relative orbit control design for the PRISMA formation flying mission," *AIAA Guidance, Navigation, and Control Conference and Exhibit*, August 21-24 2006.

[14] T. Bennett and H. Schaub, "Continuous-Time Modeling and Control Using Linearized Relative Orbit Elements," *AAS/AIAA Astrodynamics Specialists Conference*, Vail, CO, August 9-13 2015.

[15] O. Montenbruck, "An epoch state filter for use with analytical orbit models of low earth satellites," *Aerospace Science and Technology*, 2000, pp. 277–287.

[16] F. L. Markley and J. R. Carpenter, "Linear Covariance Analysis and Epoch State Estimators," *NASA Goddard Space Flight Center*.

[17] D. C. Woffinden and D. K. Geller, "Observability Criteria for Angles-Only Navigation," *IEEE Transactions on Aerospace and Electronic Systems*, Vol. 45, July 2009.

[18] J. Tombasco and P. Axelrad, "Along-Track Separation Uncertainty Modeling Given Space-Based Optical Observations," *Journal of Guidance, Control and Dynamics*, Vol. 35, June 2012.

[19] F. deBruijn, E. Gill, and J. How, "Comparitive Analysis of Cartesian and Curvilinear Clohessy-Wiltshire Equations," *Journal of Aerospace Engineering, Sciences and Applications*, Vol. 3, August 2011.

[20] T. Bennett and H. Schaub, "Space-to-Space Based Relative Motion Estimation Using Linearized Relative Orbit Elements," Maui, HI, Advanced Maui Optical and Space Surveillance Conference, September 15-18 2015.

[21] H. Schaub and J. L. Junkins, *Analytical Mechanics of Space Systems*. Reston, VA: AIAA Education Series, 2nd ed., October 2009.

[22] B. D. Tapley, B. E. Schutz, and G. H. Born, *Statistical Orbit Determination*. Burlington, MA: Elsevier Academic Press, 2004.

APPENDIX

Rectilinear Measurement Sensitivity

The rectilinear elevation partials are

$$H_{2,1}(t) = -z(t)\left(2x(t)\cos(nt) - 4y(t)\sin(nt)\right)/2\kappa_1\kappa_2 \tag{30a}$$
$$H_{2,2}(t) = z(t)\left(2x(t)\sin(nt) + 4y(t)\cos(nt)\right)/2\kappa_1\kappa_2 \tag{30b}$$
$$H_{2,3}(t) = \left(-z(t)(2x(t) - nty(t))\right)/2\kappa_1\kappa_2 \tag{30c}$$
$$H_{2,4}(t) = -2z(t)y(t)/2\kappa_1\kappa_2 \tag{30d}$$
$$H_{2,5}(t) = \cos(nt)/\kappa_2 \tag{30e}$$
$$H_{2,6}(t) = -\sin(nt)/\kappa_2 \tag{30f}$$

The rectilinear range partials are

$$H_{3,1}(t) = \left(x(t)\cos(nt) - 2y(t)\sin(nt)\right)/2\rho \tag{31a}$$
$$H_{3,2}(t) = \left(-x(t)\sin(nt) - 2y(t)\cos(nt)\right)/2\rho \tag{31b}$$
$$H_{3,3}(t) = \left(2x(t) - 3nty(t)\right)/2\rho \tag{31c}$$
$$H_{3,4}(t) = y(t)/\rho \tag{31d}$$
$$H_{3,5}(t) = z(t)\cos(nt)/\rho \tag{31e}$$
$$H_{3,6}(t) = -z(t)\sin(nt)/\rho \tag{31f}$$
$$\tag{31g}$$

Curvilinear Measurement Sensitivity

The curvilinear elevation partials are

$$\begin{aligned} H^{\text{curv}}_{1,1}(t) = &-\left(\cos\left(\frac{\delta s}{r_c}\right)\left[r_c x(t)\cos(nt) - 2(\delta r + r_c)y(t)\sin(nt)\right]\right. \\ &\left. + \sin\left(\frac{\delta s}{r_c}\right)\left[r_c y(t)\cos(nt) - 2(\delta r + r_c)x(t)\sin(nt)\right]\right)/r_c\kappa_2 \end{aligned} \tag{32a}$$

$$\begin{aligned} H^{\text{curv}}_{1,2}(t) = z(t)&\left(\cos\left(\frac{\delta s}{r_c}\right)\left[2(\delta r + r_c)y(t)\cos(nt) + r_c x(t)\sin(nt)\right]\right. \\ &\left. + \sin\left(\frac{\delta s}{r_c}\right)\left[r_c y(t)\sin(nt) - 2(\delta r + r_c)x(t)\cos(nt)\right]\right)/r_c\kappa_2 \end{aligned} \tag{32b}$$

$$\begin{aligned} H^{\text{curv}}_{1,3}(t) = &\left(z(t)\cos\left(\frac{\delta s}{r_c}\right)\left[3nty(t)(\delta r + r_c) - 2r_c x(t)\right]\right. \\ &\left. - z(t)\sin\left(\frac{\delta s}{r_c}\right)\left[3ntx(t)(\delta r + r_c) + 2r_c y(t)\right]\right)/2r_c\kappa_2 \end{aligned} \tag{32c}$$

$$H^{\text{curv}}_{1,4}(t) = (\delta r + r_c)z(t)\left(x(t)\sin\left(\frac{\delta s}{r_c}\right) - y(t)\cos\left(\frac{\delta s}{r_c}\right)\right)/r_c\kappa_2 \tag{32d}$$
$$H^{\text{curv}}_{2,5}(t) = \cos(nt)/\kappa_2 \tag{32e}$$
$$H^{\text{curv}}_{2,6}(t) = -\sin(nt)/\kappa_2 \tag{32f}$$